

## REPORTS

size; island size promoted abundances of some organisms and reduced others (Fig. 1). Second, our study found diversity, community composition, and ecosystem functioning all responded to island attributes. Although this work was not designed to separate the effects of diversity from those of composition on ecosystem processes, it provides strong evidence that inter-island variation in community structure is an important driver of ecosystem functioning. Finally, our results support previous suggestions (12–14) that islands can serve as useful models for better understanding the functioning of ecosystems. Although a growing number of studies have used the concepts developed in island geography for predicting the community-level attributes of both real (e.g., oceanic) islands and habitat islands resulting from habitat fragmentation (27–30), the implications of this at the ecosystem level have received surprisingly little attention. Our results provide evidence from a model system that ecosystem attributes are responsive to island biogeographic effects on community structure and that this should result in important differences in the functioning between spatially separated insular communities.

### References and Notes

- J. H. Lawton, *Oikos* **71**, 367 (1994).
- J. P. Grime, *Plant Strategies, Vegetation Processes and Ecosystem Properties* (Wiley, Chichester, UK, 2001).
- M. Loreau *et al.*, *Science* **294**, 804 (2001).
- M. Loreau, S. Naeem, P. Inchausti, Eds., *Biodiversity and Ecosystem Functioning* (Oxford Univ. Press, Oxford, 2002).
- D. A. Wardle, *Communities and Ecosystems: Linking the Aboveground and Belowground Components* (Princeton Univ. Press, Princeton, NJ, 2002).
- R. H. MacArthur, E. O. Wilson, *The Theory of Island Biogeography* (Princeton Univ. Press, Princeton, NJ, 1967).
- D. S. Simberloff, *Ecology* **57**, 629 (1976).
- M. L. Rosenzweig, *Species Diversity in Time and Space* (Cambridge Univ. Press, Cambridge, 1995).
- R. J. Whittaker, *Island Biogeography: Ecology, Evolution and Conservation* (Oxford Univ. Press, Oxford, 1998).
- T. W. Schoener, C. A. Toft, *Science* **219**, 1353 (1983).
- D. A. Spiller, T. W. Schoener, *Oikos* **78**, 15 (1997).
- P. M. Vitousek, L. L. Loope, H. Adersen, Eds., *Islands: Biological Diversity and Ecosystem Function* (Springer Verlag, Berlin, 1995).
- D. A. Wardle, *J. Biogeog.* **29**, 583 (2002).
- P. M. Vitousek, *J. Biogeog.* **29**, 573 (2002).
- D. A. Wardle, O. Zackrisson, G. Hörnberg, C. Gallet, *Science* **277**, 1296 (1997).
- W. B. Anderson, G. A. Polis, *Oecologia* **118**, 324 (1999).
- N. M. Nadkarni, *Am. Zool.* **34**, 70 (1994).
- B. A. Richardson, M. J. Richardson, F. N. Scatena, W. H. McDowell, *J. Trop. Ecol.* **16**, 167 (2000).
- P. Armbruster, R. A. Hutchinson, P. Cotgreave, *Oikos* **96**, 225 (2002).
- Methods and materials are available as supporting evidence on Science Online.
- A. Moeed, M. J. Meads, *N. Z. J. Ecol.* **6**, 39 (1983).
- For each of the two studies,  $R^2$  values were determined across all the epiphytes between each response variable depicted in Figs. 1 and 2 and a range of descriptive variables, namely, diameter at 1.3-m height of the tree hosting the epiphyte, diameter of branch hosting the epiphyte, the direct distance of the epiphyte from the ground, the direct distance of the epiphyte to the three nearest epiphytes, the diameters of the three nearest epiphytes, and the cumulative distance along branch-
- and trunks between the epiphyte and both the ground and the three nearest epiphytes (20). Of the 422  $R^2$  values determined, around 5% of values were significantly different from 0 at  $P = 0.05$  as expected by chance, and only two were significant at  $P = 0.001$ . These were both for the observational experiment, i.e., between populations of predatory nematodes and tree diameter ( $R^2 = 0.174$ ), and between populations of Formicidae and branch diameter ( $R^2 = 0.243$ ).
- J. M. Levine, *Science* **288**, 852 (2000).
- Island size class did not significantly affect concentrations in harvested epiphytes of foliar N [ $F(2,52) = 0.37$ ,  $P = 0.691$ ] or P [ $F(2,52) = 1.83$ ,  $P = 0.170$ ], but did affect concentrations of root N [ $F(2,47) = 4.36$ ,  $P = 0.018$ ] and root P [ $F(2,47) = 5.65$ ,  $P = 0.006$ ]. The mean root P concentration was 17% greater in the small than in the large islands, whereas root N was 7% greater in the large than in the small islands.
- For the observational study, humus gravimetric moisture concentration at harvest was significantly related to island size [ $F(2,51) = 4.59$ ,  $P = 0.015$ ], but not tree species [ $F(2,51) = 0.36$ ,  $P = 0.694$ ]. The mean moisture concentration was 28% greater in the large than in the small islands. For the experimental study, moisture concentration did not show a significant relationship with either island size [ $F(2,40) = 2.33$ ,  $P = 0.110$ ] or tree species [ $F(2,40) = 1.16$ ,  $P = 0.324$ ]. Greater reduction of variation of soil moisture concentration across island size classes was possible for the experimental than for the observational study, because experimental islands were constructed to be the same depth regardless of diameter, so that regardless of island size the interior of each island was 35 mm from the surface.
- H. Setälä, *Ecol. Res.* **17**, 207 (2002).
- A. Gonzales, J. H. Lawton, F. S. Gilbert, T. M. Blackburn, I. Evans-Freke, *Science* **281**, 2045 (1998).
- A. Gonzales, E. J. Chaneton, *J. Anim. Ecol.* **71**, 594 (2002).
- S. K. Collinge, *Ecology* **81**, 2211 (2000).
- T. Tscharnke, I. Steffan-Dewenter, A. Kruess, C. Thies, *Ecol. Appl.* **12**, 354 (2002).
- We thank R. Buxton and C. Watt for technical help; B. and A. Renton and C. Macleod for the use of their land for this study; and D. Peltzer, H. Setälä, and three anonymous reviewers for helpful comments on the manuscript. This work was supported by the New Zealand Marsden Fund.

### Supporting Online Material

www.sciencemag.org/cgi/content/full/301/5640/1717/DC1

Materials and Methods  
References and Notes

9 June 2003; accepted 14 July 2003

# Bidirectional Transmembrane Signaling by Cytoplasmic Domain Separation in Integrins

Minsoo Kim,\* Christopher V. Carman,\* Timothy A. Springer†

Although critical for development, immunity, wound healing, and metastasis, integrins represent one of the few classes of plasma membrane receptors for which the basic signaling mechanism remains a mystery. We investigated cytoplasmic conformational changes in the integrin LFA-1 ( $\alpha_L\beta_2$ ) in living cells by measuring fluorescence resonance energy transfer between cyan fluorescent protein–fused and yellow fluorescent protein–fused  $\alpha_L$  and  $\beta_2$  cytoplasmic domains. In the resting state these domains were close to each other, but underwent significant spatial separation upon either intracellular activation of integrin adhesiveness (inside-out signaling) or ligand binding (outside-in signaling). Thus, bidirectional integrin signaling is accomplished by coupling extracellular conformational changes to an unclasp and separation of the  $\alpha$  and  $\beta$  cytoplasmic domains, a distinctive mechanism for transmitting information across the plasma membrane.

Signaling across the cell membrane is typically accomplished by either conformational changes in receptor transmembrane domains, as in G protein–coupled receptors, or by lateral association of two or more monomers, as in receptor tyrosine kinases. Integrins represent a large family of heterodimeric receptors that have the ability to mediate bidirectional signaling. Stimuli received by cell surface receptors, including G protein–coupled chemokine receptors and tyrosine kinase–coupled T

cell receptors, initiate intracellular signals that impinge on integrin cytoplasmic domains and trigger increased adhesiveness in the extracellular domain (inside-out priming/signaling). Ligand binding by integrin extracellular domains is transduced to the cytoplasm in the classical outside-in direction to regulate intracellular signals that affect cellular growth, differentiation, and apoptosis (outside-in activation/signaling). However, the basic mechanism by which the relatively small cytoplasmic domains, which themselves lack enzymatic activity, function to receive and transmit intracellular signals remains unknown.

Activation of cell surface integrins is associated with conformational changes in the extracellular domains, as evidenced by the many monoclonal antibodies (mAbs)

CBR Institute for Biomedical Research, Department of Pathology, Harvard Medical School, 200 Longwood Avenue, Boston, MA 02115, USA.

\*These authors contributed equally to this work.

†To whom correspondence should be addressed. E-mail: springeroffice@cbr.med.harvard.edu

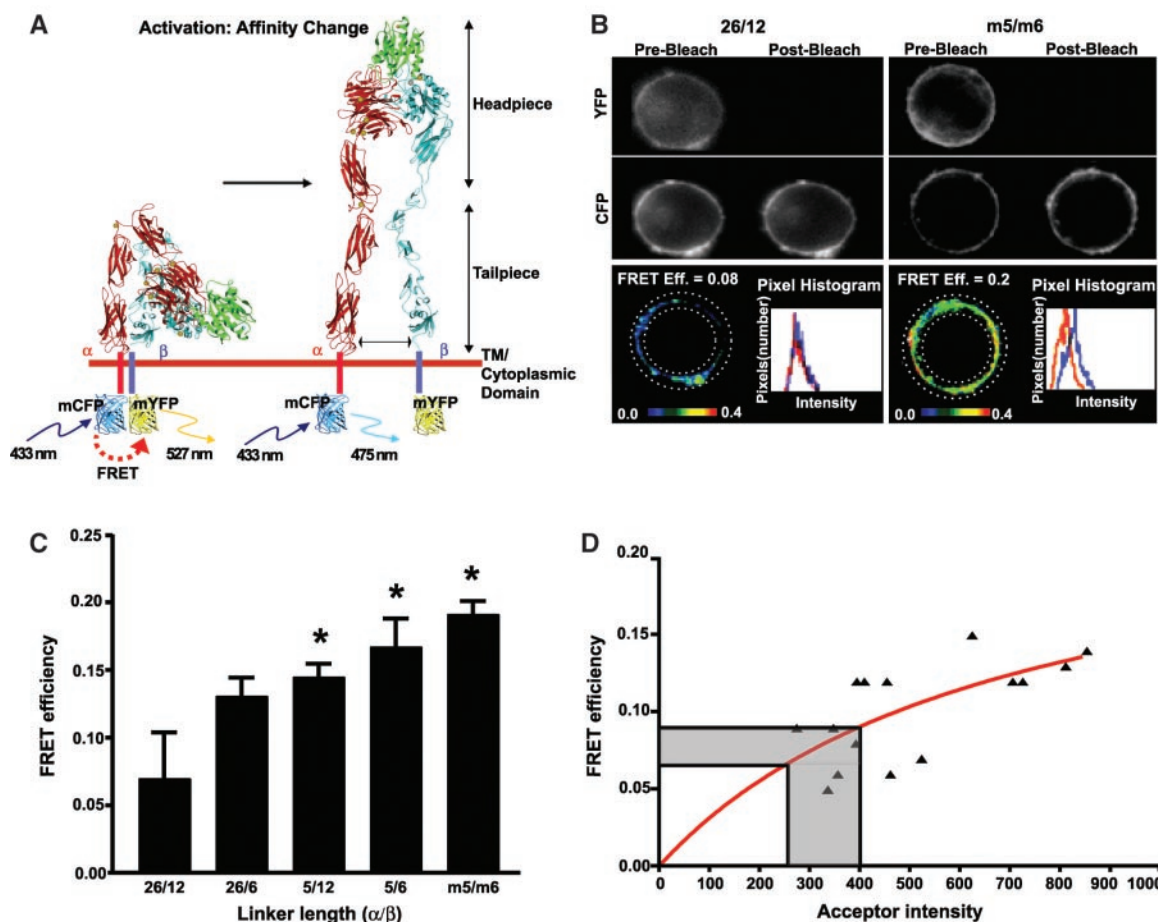
identified that bind preferentially to the activated and/or ligand-occupied forms of integrins (1). Recent nuclear magnetic resonance (NMR) (2) and electron microscopic (EM) studies (3) of purified extracellular domains have demonstrated large-scale rearrangements associated with integrin activation and ligand binding. In addition, an engineered conformational change in the ligand binding inserted (I) domain of LFA-1 ( $\alpha_L\beta_2$ ) is sufficient to drive a 10,000-fold increase in affinity for the ligand ICAM-1 (4, 5). Mutation of the membrane proximal cytoplasmic regions of the  $\alpha$  and  $\beta$  subunits induces constitutive activation (6, 7), suggesting that cytoplasmic interactions between the  $\alpha$  and  $\beta$  subunits regulate the affinity of integrins. Consistent with this explanation, introduction of an artificial clasp between the  $\alpha$  and  $\beta$  cytoplasmic domains constrains an integrin to

be inactive, whereas release of the clasp induces constitutive activation (8). One recent NMR study suggests a specific interaction that is disrupted by mutations and by binding of the talin head domain (9), whereas another NMR study suggested a different structure for the complex (10), and two other NMR studies have failed to detect interactions (11, 12). An EM study is consistent with association between the transmembrane domains in the detergent solubilized resting  $\alpha_{IIb}\beta_3$  (13). Thus, although specific and regulated interactions between  $\alpha$  and  $\beta$  subunit cytoplasmic domains have been widely speculated to be important for integrin activation, they have never been directly demonstrated in vivo. Here, we use fluorescence resonance energy transfer (FRET) (Fig. 1A) to investigate the spatial proximity of  $\alpha_L$  and  $\beta_2$  cytoplasmic domains in living cells. These studies

provide evidence for conformational changes in the cytoplasmic domains of integrins during physiologic activation.

In initial fusion constructs, the length of the linker between the C-terminus of  $\alpha_L$  or  $\beta_2$  and the N-terminus of cyan fluorescent protein (CFP) or yellow fluorescent protein (YFP) was varied. Combinations of these constructs with 26- or 5-residue  $\alpha$  subunit linkers and 12- or 6-residue  $\beta$  subunit linkers were transiently transfected into K562 cells, where they were distributed predominantly to the plasma membrane (Fig. 1B). Basal FRET efficiency was measured by the acceptor-photobleach method in which the donor (CFP) fluorescence intensity before and after specific photodestruction of acceptor (YFP) was compared (Fig. 1B). Gradual reduction in the total length of the  $\alpha$  and  $\beta$  subunit linkers was associated with a steady increase in FRET (Fig. 1C), suggesting that the cytoplasmic domains are basally in proximity.

**Fig. 1.** Development of the integrin cytoplasmic domain FRET assay. (A) Schematic representation of integrin activation. In the bent conformation (left), extensive interactions are present between the integrin headpiece and tailpiece, and the juxtamembrane, C-terminal segments of the  $\alpha$  and  $\beta$  subunit extracellular domains are in proximity (2, 3, 30). Proximity between CFP and YFP fused to the C-termini of the cytoplasmic domains would result in efficient FRET. In the extended integrin conformation (right), there is no interaction between the  $\alpha$  and  $\beta$  subunits in the tailpiece (2, 3). Movement apart of  $>100$  Å of mCFP and mYFP would abolish FRET. Ribbon diagrams are based on crystal and negative stain EM studies of integrin  $\alpha_v\beta_3$  (3, 30) (red and blue), and crystal studies on integrin I domains (7) (green) and GFP (37) (cyan for CFP and yellow for YFP). The orientation between these units is arbitrary. (B and C). Intersubunit FRET measurements. (B) Images of CFP and YFP fluorescence for individual cells before and after YFP bleaching are shown in the upper two rows. Note disappearance of YFP fluorescence after bleaching, the marked increase in CFP fluorescence for m5/m6, and little increase for 26/12. In the lower row, FRET efficiency from 0 (black) to 0.4 (red) is shown for each pixel in the region of interest on the plasma membrane of the cell. Pixel intensity histograms are for each CFP pixel acquired before (red line) and after (blue line) photobleaching the YFP acceptor. (C) Basal intersubunit FRET efficiency. \*,  $P < 0.05$  versus 26/12 ( $n = 7$  to 12 cells with acceptor intensity of 250 to 400). Bars show SEM. (D) Interheterodimer FRET between neighboring  $\alpha_L/\beta_2$



molecules for individual cells (triangles) was fit to the saturable one-site binding model  $E\% = E\%_{max}F/(F + K)$ , where FRET efficiency ( $E\%$ ) is a hyperbolic function of the YFP acceptor intensity ( $F$ ), and  $K$  is analogous to a dissociation constant (14). The nonlinear least squares regression fits of FRET efficiency between  $\alpha_L$ -mCFP/ $\beta_2$  and  $\alpha_L$ -mYFP/ $\beta_2$  (red curve) yielded  $K = 700$ , showing little association. By contrast, cross-linking with TS2/4 mAb and anti-IgG for 30 min at 37° C yielded  $K = 10.4$ , showing association between heterodimers. The grey region shows the range of acceptor intensity of cells that were selected for all subsequent intersubunit FRET measurements and the corresponding background values expected for interheterodimer FRET.

## REPORTS

Constructs containing linkers between  $\alpha_L$  and CFP and between  $\beta_2$  and YFP of 5 and 6 residues, respectively, exhibited the highest FRET efficiency. Mutations were then introduced into CFP and YFP that inhibit their inherent tendency to form hetero- or homodimers, generating “monomeric” CFP (mCFP) and YFP (mYFP) (14). Basal FRET efficiency for  $\alpha_L$ -CFP/ $\beta_2$ -YFP and  $\alpha_L$ -mCFP/ $\beta_2$ -mYFP heterodimers was similar (5/6 compared with m5/m6, Fig. 1C), and the  $\alpha_L$ -mCFP and  $\beta_2$ -mYFP constructs containing 5- and 6-residue linkers were used for most subsequent experiments.

To address the potential contribution of interheterodimer energy transfer to our measurement of intersubunit FRET, we transiently transfected cells with  $\alpha_L$ -mYFP and  $\alpha_L$ -mCFP, together with wild-type  $\beta_2$ , and measured energy transfer between  $\alpha_L$ -mYFP/ $\beta_2$  and  $\alpha_L$ -mCFP/ $\beta_2$  over a range of cell surface densities as determined by acceptor intensities. Interheterodimer energy

transfer increased with increasing integrin density at the cell surface (Fig. 1D). Fitting the data to a previously described equation (Fig. 1D, red line) (14) showed little tendency of  $\alpha_L\beta_2$  heterodimers to associate or cluster in the membrane. At relatively low density (acceptor intensities from 250 to 400 arbitrary fluorescence units), energy transfer efficiency between  $\alpha_L$ -mYFP/ $\beta_2$  and  $\alpha_L$ -mCFP/ $\beta_2$  was  $\sim 0.07$ . However, FRET efficiency between  $\alpha_L$ -CFP and  $\beta_2$ -YFP (5/6) or  $\alpha_L$ -mCFP and  $\beta_2$ -mYFP (m5/m6), measured in the same range of acceptor intensity between 250 and 400, was 0.17 to 0.2 (Fig. 1C), demonstrating that this energy transfer occurs primarily through intersubunit FRET within individual heterodimers. All subsequent FRET measurements were made on cells with acceptor intensities of 250 to 400.

Stable K562 cell transfectants expressing  $\alpha_L$ -mCFP/ $\beta_2$ -mYFP and  $\alpha_L$ -CFP/ $\beta_2$ -YFP were

generated, and clones expressing acceptor intensity ranging from 250 to 400 units were selected. Most of the LFA-1 in these cells, as with the transient transfectants, was distributed to the plasma membrane (Fig. 2A). Some Golgi fluorescence was also evident, but was omitted by measuring FRET only in the rim around each cell. SDS-polyacrylamide gel electrophoresis (SDS-PAGE) of cell lysates of the stable transfectants and Western blotting demonstrated that both  $\alpha_L$ -CFP and  $\beta_2$ -YFP were increased in  $M_r$  compared with wild-type  $\alpha_L$  and  $\beta_2$  (Fig. 2B, left and center) by an amount corresponding to the  $M_r$  of the fused CFP or YFP.  $\alpha_L$ -CFP and  $\beta_2$ -YFP were also recognized by anti-green fluorescent protein (GFP), which cross-reacts with CFP and YFP (Fig. 2B, right). No evidence of proteolytic cleavage of CFP or YFP was detected (Fig. 2B, right). Clones expressing similar levels of cell surface  $\alpha_L$ -CFP/ $\beta_2$ -YFP,  $\alpha_L$ -mCFP/ $\beta_2$ -mYFP, and wild-type  $\alpha_L/\beta_2$  were selected (Fig. 2C).

The fusion constructs were tested for functional responses. The wild-type  $\alpha_L/\beta_2$ ,  $\alpha_L$ -mCFP/ $\beta_2$ -mYFP, and  $\alpha_L$ -CFP/ $\beta_2$ -YFP transfectants showed low basal adhesion to the immobilized ligand ICAM-1 (Fig. 2D) and low basal staining with KIM127 (Fig. 2E), a mAb that binds near the genuflection in the  $\beta_2$  subunit and reports the active, extended conformation of LFA-1 (2, 15, 16). In cells expressing wild-type  $\alpha_L/\beta_2$  and  $\alpha_L$ -mCFP/ $\beta_2$ -mYFP, ICAM-1 binding and KIM127 staining were greatly increased by  $Mn^{2+}$  (17, 18), CBR LFA-1/2, an activating mAb to  $\beta_2$  (15), and phorbol 12-myristate 13-acetate (PMA) (19) (Fig. 2D and E). By contrast, cells expressing  $\alpha_L$ -CFP/ $\beta_2$ -YFP, containing the dimerizing form of CFP and YFP, bound less efficiently to ICAM-1 when activated by  $Mn^{2+}$  and CBR LFA-1/2, and binding could not be activated by PMA (Fig. 2D). In addition, PMA was less effective than  $Mn^{2+}$  in enhancing KIM127 staining in  $\alpha_L$ -CFP/ $\beta_2$ -YFP (Fig. 2E).

To determine whether integrin activation is associated with spatial rearrangements of the  $\alpha$  and  $\beta$  subunit cytoplasmic tails in living cells, FRET efficiency was measured on cells expressing  $\alpha_L$ -mCFP/ $\beta_2$ -mYFP and  $\alpha_L$ -CFP/ $\beta_2$ -YFP. In cells expressing  $\alpha_L$ -mCFP/ $\beta_2$ -mYFP, FRET was significantly decreased from basal levels after treatment with CBR LFA-1/2 mAb,  $Mn^{2+}$  + CBR LFA-1/2 mAb, or PMA (Fig. 3A and C). However, no significant clustering or redistribution of LFA-1 in the plasma membrane (20, 21, 22) was induced by the activating treatments used in this study (Fig. 3C); furthermore, clustering would have increased rather than decreased FRET efficiency. These results show that activation mediated by CBR LFA-1/2 mAb and PMA is associated with spatial separation of the  $\alpha_L$  and  $\beta_2$  cytoplasmic domains. In contrast, in cells expressing  $\alpha_L$ -CFP/ $\beta_2$ -YFP,

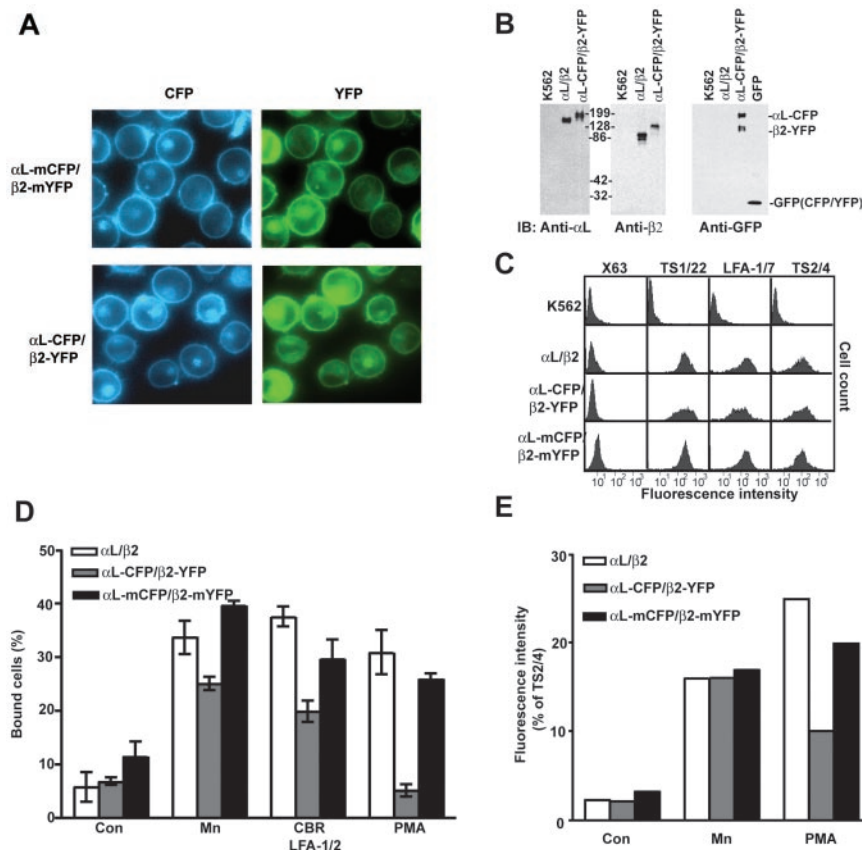


**Fig. 2.** Stable cells expressing  $\alpha_L$ -mCFP/ $\beta_2$ -mYFP preserve normal functional profiles of LFA-1. (A) Fluorescence images of stably transfected K562 cells with  $\alpha_L$ -CFP/ $\beta_2$ -YFP or  $\alpha_L$ -mCFP/ $\beta_2$ -mYFP demonstrate membrane localization of CFP and YFP signals. (B) Whole cell lysates of K562 and stable transfectants expressing wild-type  $\alpha_L/\beta_2$  or  $\alpha_L$ -CFP/ $\beta_2$ -YFP were subjected to SDS-PAGE and Western blotting with the indicated antibodies. (C) Cell surface expression levels of  $\alpha_L/\beta_2$  were determined by immunofluorescence flow cytometry on parental K562 cells or stable transfectants. mAbs TS1/22, CBR LFA-1/7, and TS2/4 recognize  $\alpha_L$ ,  $\beta_2$ , and  $\alpha_L/\beta_2$  complex, respectively. Nonbinding X63 IgG1 was used as negative control. (D) Adhesion to immobilized ICAM-1. K562 transfectants were allowed to bind ICAM-1-coated substrates without stimulation [control (Con)] or after stimulation with 1 mM  $Mn^{2+}$ , 10  $\mu$ g/ml CBR LFA-1/2 mAb, or 100 nM PMA. Data are mean  $\pm$  SEM for one representative experiment in triplicate. (E) KIM127 activation epitope induction by  $Mn^{2+}$  or PMA.

CBR LFA-1/2 mAb and PMA did not alter FRET efficiency (Fig. 3B). These results are explained by the previous observations that CFP and YFP, but not mCFP and mYFP, mediate dimerization when membrane-associated (14), and that an association enforced by substitution of integrin  $\alpha$  and  $\beta$  subunit cytoplasmic domains with  $\alpha$ -helical coiled-coil domains blocks activation (8). Thus, the results suggest that in  $\alpha_L$ -CFP/ $\beta_2$ -YFP, CFP and YFP form a heterodimer that opposes cytoplasmic domain separation and perturbs normal integrin activation. By contrast,  $\alpha_L$ -mCFP/ $\beta_2$ -mYFP functions indistinguishably from wild-type  $\alpha_L\beta_2$ .  $Mn^{2+}$  had no effect on FRET in either  $\alpha_L$ -mCFP/ $\beta_2$ -mYFP or  $\alpha_L$ -CFP/ $\beta_2$ -YFP transfectants (Fig. 3, A and B), in contrast with its activation of KIM127 epitope exposure and adhesion (Fig. 2E). This result suggests that  $Mn^{2+}$ -mediated activation can take place independently of  $\alpha_L$  and  $\beta_2$  cytoplasmic domain separation.

Binding to ligands by integrins transduces signals into cells. Electron micrographic studies of the extracellular fragment of  $\alpha_v\beta_3$  integrin show that binding to ligand-mimetic cyclic Arg-Gly-Asp (RGD) peptides shifts the conformational equilibrium completely toward the extended form with the open headpiece, which has widely separated C-terminal juxtamembrane domains, whereas  $Mn^{2+}$  shifts the equilibrium only partially, so that the bent conformation and extended conformations with open and closed headpieces coexist (3). The presence of transmembrane and cytoplasmic domains would affect the conformational equilibrium. To examine the effect of ligand binding on cytoplasmic domain association, we incubated cells with soluble ICAM-1 in the presence of  $Mn^{2+}$ , which increases the affinity of LFA-1 sufficiently to obtain appreciable binding to soluble ICAM-1 (17), and compared the results with results in  $Mn^{2+}$  alone. Binding of soluble ICAM-1 to  $\alpha_L$ -mCFP/ $\beta_2$ -mYFP in the presence of  $Mn^{2+}$  induced a significant increase in KIM127 staining compared with  $Mn^{2+}$  alone (not shown) and a dramatic decrease in FRET efficiency compared with cells treated with  $Mn^{2+}$  alone (Fig. 3A). This result shows that ligand binding induces spatial separation of the cytoplasmic domains and defines a key step in outside-in signal transduction.

Mutation of the conserved GFFKR sequence at the boundary between the integrin  $\alpha$  subunit transmembrane and cytoplasmic domains results in constitutive adhesiveness (6, 7) as well as increased exposure of extracellular domain activation epitopes (7), suggesting that the GFFKR sequence stabilizes the inactive integrin conformation. Thus, the GFFKR motif of  $\alpha_L$ -mCFP was mutated to GAAKR, and K562 cells were transiently transfected with

this construct and  $\beta_2$ -mYFP. FRET efficiency measured under basal conditions was significantly decreased compared with  $\alpha_L$ -mCFP/ $\beta_2$ -mYFP transfectants (Fig. 3D). Thus, constitutive activation induced by perturbation of the  $\alpha$  subunit GFFKR sequence is associated with basal spatial separation of the  $\alpha$  and  $\beta$  subunit cytoplasmic domains.

Talin is a 250-kD cytoskeletal protein that is composed of a 47-kD N-terminal head domain and a 190-kD C-terminal rod domain. When freed from association with the rod domain by proteolysis or truncation, the talin head domain activates integrin  $\alpha_{IIb}\beta_3$  (9, 23, 24). Talin binds directly to  $\beta_1$ ,  $\beta_2$ , and  $\beta_3$  integrins (25), but whether it activates  $\beta_2$  integrins has not been examined.  $\alpha_L$ -mCFP/ $\beta_2$ -mYFP K562 transfectants were further transfected with hemagglutinin (HA) tagged talin head domain (TH), and clones expressing no (TH null), medium (TH middle), or high (TH high) levels of talin head domain were selected (Fig. 4A). Expression of the talin head domain did not change the surface expression or distribution pattern of  $\alpha_L$ -mCFP/ $\beta_2$ -mYFP. Immunoprecipitation with

CBR LFA-1/2 mAb to the  $\beta_2$  subunit followed by immunoblotting with HA antibody showed that the talin head domain associated with LFA-1 (Fig. 4B). Basal adhesiveness to immobilized ICAM-1 was significantly enhanced in cells expressing middle and high levels of talin head domain (Fig. 4C), demonstrating that the talin head domain activates  $\alpha_L\beta_2$ , as previously shown for  $\alpha_{IIb}\beta_3$  (9, 23, 24). In contrast, TH null cells behaved similarly to parental  $\alpha_L$ -mCFP/ $\beta_2$ -mYFP cells (Fig. 4C). Basal FRET efficiency in talin head domain transfectants revealed significant decreases in energy transfer between  $\alpha_L$ -mCFP and  $\beta_2$ -mYFP, which were proportional to the level of talin head domain expression (Fig. 4D). These data demonstrate that talin head domain binding to  $\alpha_L\beta_2$  causes a spatial separation of the cytoplasmic domains, consistent with NMR studies on dissociation, by talin head domain, of  $\alpha_{IIb}\beta_3$  cytoplasmic complex (9).

Physiologic regulation of integrins can occur through a variety of cell surface receptors. One of the best characterized examples is activation of integrin-dependent leukocyte ar-

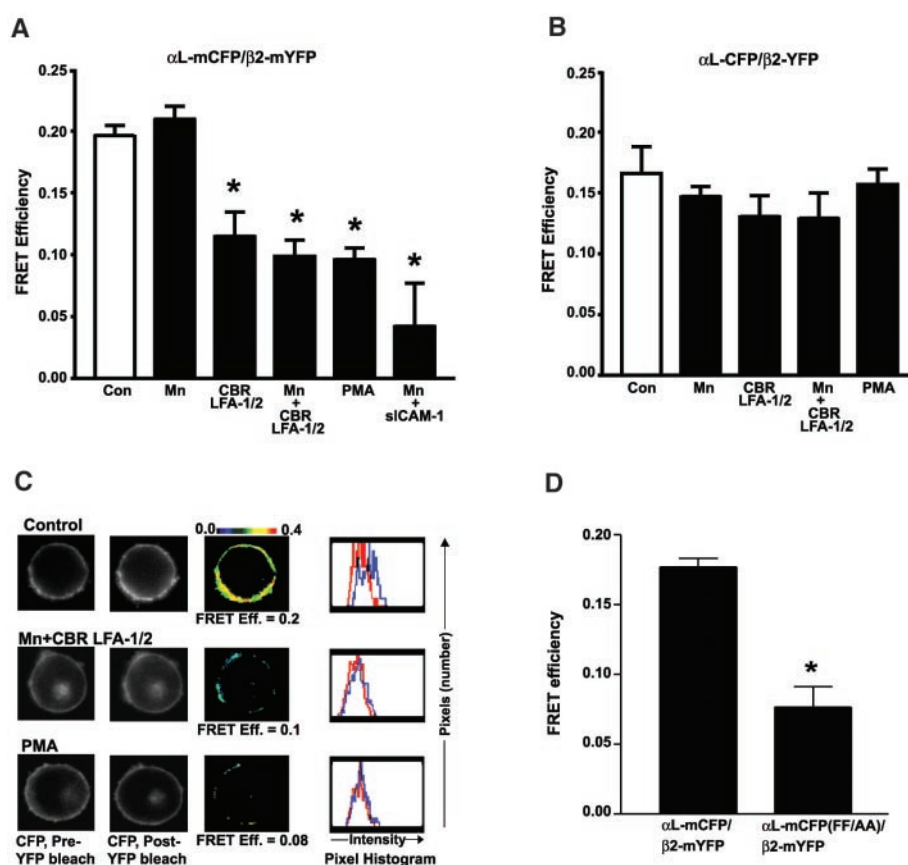


**Fig. 3.** Activation of  $\alpha_L$ -mCFP/ $\beta_2$ -mYFP causes spatial separation of the cytoplasmic domains. (A and B) FRET was measured in  $\alpha_L$ -mCFP/ $\beta_2$ -mYFP (A) or  $\alpha_L$ -CFP/ $\beta_2$ -YFP (B) K562 transfectants after the indicated treatment. Data are averages  $\pm$  SEM for 5 to 10 cells. \*,  $P < 0.05$  versus control (Con). (C) Representative single-cell FRET measurements. Note the greater post-YFP bleach increase in CFP fluorescence for the control cell. Data are displayed as in Fig. 1B, except only CFP fluorescence is shown. (D) Effect of GFFKR motif mutation on FRET. Data show mean  $\pm$  SEM for 4 to 10 cells. \*,  $P < 0.05$  versus  $\alpha_L$ -mCFP/ $\beta_2$ -mYFP.

REPORTS

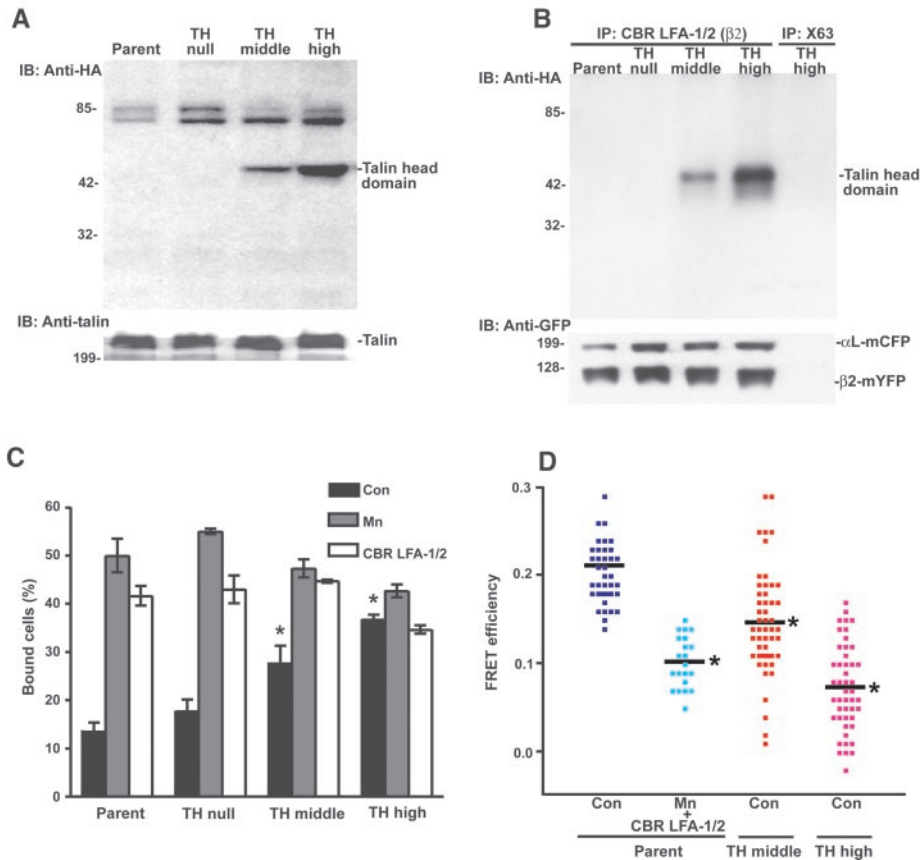
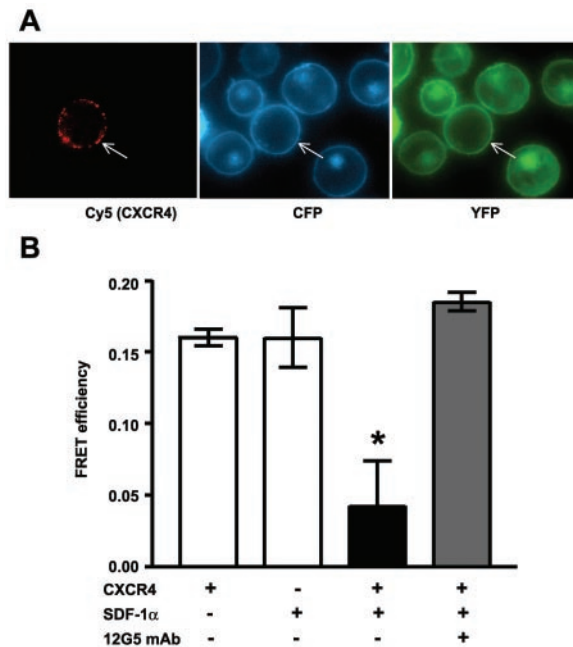


**Fig. 4.** Effect of the talin head domain on integrin LFA-1 cytoplasmic domain association and adhesion to ICAM-1. All experiments are on cells expressing  $\alpha_L$ -mCFP/ $\beta_2$ -mYFP and different amounts of the N-terminally HA-tagged talin head domain. (A) Talin head domain expression. Cells were subjected to SDS-PAGE and Western blotting. Blots were probed with antibody to HA (upper), then stripped and reprobed with a mAb specific for the talin rod domain. (B) Binding of the talin head domain to LFA-1. Triton X-100 lysates were immunoprecipitated with CBR LFA-1/2 mAb to  $\beta_2$  or X63 IgG1 as negative control, and subjected to SDS-PAGE and Western blotting with antibody to HA (upper), then stripped and reprobed with GFP antibody (lower). (C) Adhesion of transfectants to ICAM-1 substrates was measured in the presence of Mn<sup>2+</sup> or CBR LFA-1/2 mAb. Data are mean  $\pm$  SEM for three to six experiments, each in triplicate. \*,  $P < 0.05$  versus parental control. (D) FRET in talin head domain transfectants. Each square represents FRET efficiency of one cell. Bar = mean. \*,  $P < 0.05$  versus parental control.

**Fig. 5.** Effect of chemokine-receptor activation on LFA-1 cytoplasmic domain FRET. (A) Cells expressing  $\alpha_L$ -mCFP/ $\beta_2$ -mYFP were transiently transfected with N-terminally HA-tagged CXCR4 receptor. Transfectants were identified by staining with mouse antibody to HA and Cy5-anti-mouse Ig (arrow). (B) Effect of SDF-1 treatment on FRET. Transfectants with or without pretreatment with 10  $\mu$ g/ml 12G5 mAb were treated with or without 1  $\mu$ g/ml SDF-1 $\alpha$ . FRET was measured both on transfectants that expressed (+) or did not express (-) CXCR4, as shown with Cy5 fluorescence. \*,  $P < 0.05$  versus untreated CXCR4 transfectants. Data are mean  $\pm$  SEM for four cells.



rest and migration through G protein-coupled receptors for chemokines (26–28). To assess the effect of chemokine receptor signaling on the conformation of integrin cytoplasmic domains,  $\alpha_L$ -mCFP/ $\beta_2$ -mYFP transfectants were further transfected transiently with HA-tagged CXCR4. CXCR4 is the receptor for the chemokine SDF-1. Both cells that were positive and cells that were negative for CXCR4 expression were identified by immunofluorescence with an antibody to HA and Cy5-labeled anti-Ig (Fig. 5A). Addition of the chemokine SDF-1 significantly reduced FRET between  $\alpha_L$ -mCFP and  $\beta_2$ -mYFP in cells expressing CXCR4 but had no effect on cells lacking CXCR4 expression (Fig. 5B). Furthermore, treatment with 12G5, a blocking antibody to CXCR4, abolished the effect of SDF-1 on FRET efficiency (Fig. 5B). This result demonstrates that physiological “inside-out” activation of integrins stimulated by chemokine receptors is associated with spatial separation of the  $\alpha$  and  $\beta$  cytoplasmic domains of LFA-1.

Integrins are exceptional among regulated cell surface receptors in that the large size of their extracellular domains requires that conformational information travel great distances to couple extracellular ligand binding to the intracellular cytoplasmic domains. The problem of how to transmit information between the membrane and the ligand binding site, which are  $>200$  Å apart in the extended conformation, is in part solved by equilibration with a bent conformer, which has an  $\alpha\beta$  interface close to the membrane (3). However, the mechanism by which information flows bidirectionally across the plasma membrane in integrins has remained a mystery. The results presented here demonstrate conformational changes in integrin cytoplasmic domains associated with activation in living cells. Because many of the stimuli studied here reduced  $\alpha_L$ - $\beta_2$  FRET to a level similar to that of the measured background interheterodimer  $\alpha_L$ - $\alpha_L$  FRET, and interheterodimer FRET will still be present after maximal  $\alpha_L$ - $\beta_2$  separation, separation appears to approach the detection limit for CFP-YFP FRET of  $\sim 100$  Å. Orientation is highly unlikely to influence FRET between  $\alpha_L$ -mCFP and  $\beta_2$ -YFP because of the flexibility of the 5- and 6-residue GPVAT and GGPVAT linkers. Our studies with probes attached to the C-termini of the short integrin  $\alpha_L$  and  $\beta_2$  cytoplasmic domains do not define the nature of coupled movements in the  $\alpha_L$  and  $\beta_2$  transmembrane domains; nonetheless, the large changes in FRET that are observed appear more consistent with the most dramatic model of alterations in the transmembrane domain association, i.e., movement apart in the plane of the membrane with complete separation of the transmembrane domain (3, 8, 29), rather than with more subtle models of hinging or pistonlike motions.

We conclude that integrin priming stemming from chemokine receptor–stimulated inside-out signaling, talin head domain binding, PMA, or GFFKR mutation is associated with a significant spatial separation of the  $\alpha$  and  $\beta$  subunit cytoplasmic domains (Fig. 1A). Furthermore, outside-in signals transmitted after ligand binding also induce separation of the cytoplasmic domains. Thus, in integrin signaling across the plasma membrane, spatial separation of cytoplasmic domains is coupled to extracellular conformational change, and these mechanisms operate in both the inside-out and outside-in directions. This result demonstrates a distinctive mechanism for transmission of information across the plasma membrane by cell surface receptors.

#### References and Notes

- M. Shimaoka, J. Takagi, T. A. Springer, *Annu. Rev. Biophys. Biomol. Struct.* **31**, 485 (2002).
- N. Beglova, S. C. Blacklow, J. Takagi, T. A. Springer, *Nat. Struct. Biol.* **9**, 282 (2002).
- J. Takagi, B. M. Petre, T. Walz, T. A. Springer, *Cell* **110**, 599 (2002).
- M. Shimaoka *et al.*, *Proc. Natl. Acad. Sci. U.S.A.* **98**, 6009 (2001).
- C. Lu *et al.*, *Proc. Natl. Acad. Sci. U.S.A.* **98**, 2387 (2001).
- P. E. Hughes *et al.*, *J. Biol. Chem.* **271**, 6571 (1996).
- C. Lu, T. A. Springer, *J. Immunol.* **159**, 268 (1997).
- C. Lu, J. Takagi, T. A. Springer, *J. Biol. Chem.* **276**, 14642 (2001).
- O. Vinogradova *et al.*, *Cell* **110**, 587 (2002).
- A. M. Weljie, P. M. Hwang, H. J. Vogel, *Proc. Natl. Acad. Sci. U.S.A.* **99**, 5878 (2002).
- R. Li *et al.*, *Proc. Natl. Acad. Sci. U.S.A.* **98**, 12462 (2001).
- T. S. Ulmer, B. Yaspan, M. H. Ginsberg, I. D. Campbell, *Biochemistry* **40**, 7498 (2001).
- B. D. Adair, M. Yeager, *Proc. Natl. Acad. Sci. U.S.A.* **99**, 14059 (2002).
- D. A. Zacharias, J. D. Violin, A. C. Newton, R. Y. Tsien, *Science* **296**, 913 (2002).
- C. Lu, M. Ferzly, J. Takagi, T. A. Springer, *J. Immunol.* **166**, 5629 (2001).
- C. Lu, M. Shimaoka, Q. Zang, J. Takagi, T. A. Springer, *Proc. Natl. Acad. Sci. U.S.A.* **98**, 2393 (2001).
- I. Dransfield, C. Cabañas, A. Craig, N. Hogg, *J. Cell Biol.* **116**, 219 (1992).
- B. Leitinger, A. McDowall, P. Stanley, N. Hogg, *Biochim. Biophys. Acta* **1498**, 91 (2000).
- M. L. Dustin, T. A. Springer, *Nature* **341**, 619 (1989).
- M. Stewart, N. Hogg, *J. Cell. Biochem.* **61**, 554 (1996).
- M. Lub *et al.*, *Mol. Biol. Cell* **8**, 719 (1997).
- R. Li *et al.*, *Science* **300**, 795 (2003).
- D. A. Calderwood *et al.*, *J. Biol. Chem.* **274**, 28071 (1999).
- D. A. Calderwood *et al.*, *J. Biol. Chem.* **277**, 21749 (2002).
- S. Liu, D. A. Calderwood, M. H. Ginsberg, *J. Cell Sci.* **113**, 3563 (2000).
- M. B. Lawrence, T. A. Springer, *Cell* **65**, 859 (1991).
- J. J. Campbell *et al.*, *Science* **279**, 381 (1998).
- G. Constantin *et al.*, *Immunity* **13**, 759 (2000).
- J. Takagi, H. P. Erickson, T. A. Springer, *Nature Struct. Biol.* **8**, 412 (2001).
- J.-P. Xiong *et al.*, *Science* **294**, 339 (2001).
- F. Yang, L. G. Moss, G. N. Phillips Jr., *Nat. Biotechnol.* **14**, 1246 (1996).
- We thank A. Salas and W. Yang for purified intact and soluble ICAM-1, R. Hynes for talin cDNA, and J. Benovic for the HA-CXCR4 construct. This work was supported by NIH grant CA31798 (T.A.S.) and American Heart Association fellowship 20188T (C.V.C.).

#### Supporting Online Material

www.sciencemag.org/cgi/content/full/301/5640/1720/DC1

Materials and Methods  
References

5 March 2003; accepted 1 June 2003

## A Zinc Clasp Structure Tethers Lck to T Cell Coreceptors CD4 and CD8

Peter W. Kim,<sup>1,2</sup> Zhen-Yu J. Sun,<sup>2</sup> Stephen C. Blacklow,<sup>3</sup> Gerhard Wagner,<sup>2</sup> Michael J. Eck<sup>1,2\*</sup>

The T cell coreceptors CD4 and CD8 both associate via their cytoplasmic tails with the N-terminus of the Src-family tyrosine kinase Lck. These interactions require zinc and are critical for T cell development and activation. We examined the folding and solution structures of ternary CD4-Lck-Zn<sup>2+</sup> and CD8 $\alpha$ -Lck-Zn<sup>2+</sup> complexes. The coreceptor tails and the Lck N-terminus are unstructured in isolation but assemble in the presence of zinc to form compactly folded heterodimeric domains. The cofolded complexes have similar "zinc clasp" cores that are augmented by distinct structural elements. A dileucine motif required for clathrin-mediated endocytosis of CD4 is masked by Lck.

The Src-family tyrosine kinase Lck transduces signals that are required for normal T lymphocyte development and for antigen-dependent activation of mature T cells. Lck associates noncovalently via its N-terminal region with the cytoplasmic tails of the T cell coreceptors CD4 or CD8 $\alpha$  (1–6). Early in T cell maturation, Lck drives progression of thymocytes to the CD4+/CD8+ double-positive stage (7), but association of Lck with coreceptor is not required (8). Conversely, Lck must associate with either

CD4 or CD8 $\alpha$  to promote further progression to the mature CD4+/CD8– or CD4–/CD8+ single-positive stage (8). Furthermore, association of Lck with coreceptor is required for efficient antigen-induced T cell activation (9, 10). Lck is recruited to the activated T cell receptor (TCR) complex by its association with the cytoplasmic tails of CD4 or CD8 $\alpha$ , and it phosphorylates the TCR- $\zeta$  chain (11). Following T cell activation, Lck dissociates from CD4, and CD4 is internalized (12–16).

The domain structure of Lck, like all Src-family kinases, consists of regulatory SH3 and SH2 domains followed by the tyrosine kinase domain and a short C-terminal tail. Lck and other Src kinases are all myristoylated but otherwise share no obvious similarity in their 50 to 80 N-terminal residues. The function of this "unique" domain is unclear for most members of the family, but in Lck it mediates association

with the cytoplasmic tails of CD4 and CD8 $\alpha$  (1, 2, 6). Conserved cysteine motifs within the coreceptor tails (a CxCP motif in CD4 and CD8 $\alpha$ ) and the Lck unique domain (a CxxC motif) direct high-affinity binding (4, 5). These four conserved cysteine residues (two from Lck and two from either of the coreceptors) are hypothesized to coordinate a Zn<sup>2+</sup> ion that is critical for complex formation (17, 18). Aside from the conserved cysteine motif, the CD4 and CD8 $\alpha$  cytoplasmic tails share little sequence similarity. Although crystal structures are available for the extracellular portions of the coreceptors and for the SH3, SH2, and kinase domains of Lck, the unique region of Lck and its CD4 and CD8 $\alpha$  complexes have not been structurally characterized. To understand how both coreceptors recognize Lck and to illuminate the structural basis for regulation of CD4 internalization, we determined the structure of CD4-Lck-Zn<sup>2+</sup> and CD8 $\alpha$ -Lck-Zn<sup>2+</sup> complexes.

Based on reported structure-function studies (4, 5, 19) and preliminary nuclear magnetic resonance (NMR) analysis of the full-length coreceptor tails and Lck unique region (20), the following peptides were selected for structural analysis: (i) CD4-38, encompassing residues 396 to 433 of human CD4 (the complete cytoplasmic tail), (ii) CD8 $\alpha$ -19, corresponding to residues 189 to 207 of human CD8 $\alpha$  (lacking only the C-terminal 8 residues of the CD8 $\alpha$  cytoplasmic region), and (iii) Lck-29, encompassing residues 7 to 35 of human Lck (fig. S1). Unlabeled and uniformly <sup>15</sup>N- and/or <sup>13</sup>C-labeled CD4, CD8 $\alpha$ , and Lck peptides were prepared with a bacterial expression system (21). Two-dimensional <sup>15</sup>N-<sup>1</sup>H HSQC (heteronuclear single-quantum coherence) spectra for isolated CD4 and Lck are shown in Fig. 1 (and for CD8 $\alpha$  in fig. S2). All three spectra revealed

<sup>1</sup>Department of Cancer Biology, Dana-Farber Cancer Institute, Boston, MA 02115, USA. <sup>2</sup>Department of Biological Chemistry and Molecular Pharmacology, Harvard Medical School, Boston, MA 02115, USA. <sup>3</sup>Brigham and Women's Hospital and Department of Pathology, Harvard Medical School, Boston, MA 02115, USA.

\*To whom correspondence should be addressed. E-mail: eck@red.dfci.harvard.edu

**M. Kim et al.**

## **METHODS**

### **Cell Culture and Transfections**

K562 human leukemia cells were cultured in RPMI 1640 supplemented with 10% fetal calf serum (FCS), 100 U/ml penicillin, and 100 g/ml streptomycin. Cells ( $2.5 \times 10^5$ /well) were seeded 1 hr before transient transfection in 24-well plates in 350 l of RPMI 1640 with 10% FCS, and transfected using SuperFect reagent (Qiagen) according to the manufacturer's instructions optimized as described (29). For stable transfection, K562 cells ( $2.5 \times 10^7$ /ml in 800 l) were transfected with a total of 100 g of expression constructs by electroporation at 250 V and 960 F using 0.4-cm path-length cuvettes (Bio-Rad). After culturing 24 h in RPMI 1640 medium with 20% FCS, cells were selected for resistance to the appropriate antibiotics (1 mg/ml G418, 200 g/ml hygromycin, or 4 g/ml puromycin). Transfectants were sorted at least two times by CFP and YFP fluorescence or immunofluorescence with mAb TS2/4 to LFA-1 and seeded at a single cell per well in 96 well plates to obtain homogeneous, stable transfectants.

### **DNA Plasmids and Constructs**

The mammalian expression vectors pEYFP-N1 and pECFP-N1(Clontech) were used to generate  $\alpha_L$ -CFP and  $\beta_2$ -YFP. For  $\alpha_L$ -CFP, wild type  $\alpha_L$  subunit cDNA in Apr<sup>M8</sup> (30) was digested with HindIII and SalI and the 1.5-kb fragment that contains bases 1-1487 of  $\alpha_L$  cDNA was inserted into pECFP to make the cloning intermediate  $\alpha_L$ (HindIII/SalI)-pECFP. To create a linker between  $\alpha_L$  and ECFP, composed of 22 residues of polyproline II helix (31) and four residues of vector linker EESSRQLPTAAPEPAKVDQDAGPVAT, PCR extension was performed with  $\alpha_L$ -Apr<sup>M8</sup> and the upstream primer corresponding to  $\alpha_L$  subunit cDNA bases 1351 to 1371 and the downstream primer 5'-TATATACCGGTCCAGCGTCTTGG TCAACCTTCGGGGTTCCGGAGCTGCAGTTGGGAGCTGGCGGCTGCTCTCTTCGTCCTTGCCACCACCACTCTC-3' containing an AgeI site. PCR product was

digested with Sall and AgeI and inserted into  $\alpha_L$ (HindIII/Sall)-pECFP to make  $\alpha_L$ -CFP(26). To create the 5 amino acid linker GPVAT in  $\alpha_L$ -CFP(5), the same method was used, except with the downstream primer 5'-TATATACCGGTCCGTCCTTGCCACCACCACTCTC-3'.

For  $\beta_2$ -YFP, PCR extensions were performed on wild type  $\beta_2$  cDNA in CDM8 (32) as a template. The upstream primer 5'-TTTAAGCTTGCCACCATGCTGGGCCTGCGC-3' with a HindIII site and the downstream primer 5'-ATATAGGTAC CAGACTCTCAGCAAACCTTGGGGTT-3' with a KpnI site were used with  $\beta_2$ -CDM8. After digestion with HindIII and KpnI, the PCR fragment was inserted into HindIII and KpnI digested pEYFP, yielding the 12 amino acid linker LVPRARDPPVAT in  $\beta_2$ -YFP(12). To create the 6 amino acid linker GGPVAT in  $\beta_2$ -YFP(6), the downstream primer 5' TATATACCG GTCCGC CACTCTCAGC AAACCTTGGGGTT-3' was used and AgeI was substituted for KpnI. Monomeric mCFP and mYFP mutants were generated by replacing Leu-221 at the crystallographic dimer interface with a Lys as described (14).

Mutant  $\alpha_L$ (F1901A/F1902A)-mCFP was constructed by overlap extension PCR. The inner complementary primers were 5'-GCTGTACAAGGTTGGTGCCGCCAAACGGAACCTGAAGG-3' and 5'-CCTTCAGGTTCCGTTTGGCGGCACCAACCTTGTACAGC-3'. The outer primers corresponded to  $\alpha$  subunit cDNA bases 1351 to 1371 and CFP cDNA bases 45 to 64. The second round PCR product was digested with Sall and AgeI, and used to replace the Sall/AgeI fragment in  $\alpha_L$ -mCFP.

The talin head domain cDNA (residues 1-435 of mouse talin) was amplified from full length talin (kindly provided by Dr. Richard Hynes, MIT, Boston, MA) and cloned into the mammalian expression vector pcDNA3.1(+). The upstream primer introduced an N-terminal hemagglutinin (HA) tag. K562 cells expressing  $\alpha_L$ -mCFP/ $\beta_2$ -mYFP were

transfected, seeded in 96 well plates, and clones were selected for resistance to both G418 and hygromycin.

### **Flow Cytometry, Immunoblotting, Immunoprecipitation, and Immunofluorescence**

Flow cytometry was as described (5, 7). mAb to LFA-1 were detected using R-phycoerythrin (PE) conjugated anti-mouse IgG.

For immunoblotting, cells ( $2 \times 10^7$  in 1 ml PBS) were mixed with an equal volume of non-reducing SDS-sample buffer, and subjected to SDS 12% PAGE. Proteins were transferred to nitrocellulose membranes (33). The  $\alpha_L$  subunit was probed with polyclonal antibody N-18 (Santa Cruz) and  $\beta$  subunit was probed with CBR LFA-1/2 mAb. GFP polyclonal antibody (Clontech) was used to blot CFP and YFP. HA-tag was probed with biotin conjugated HA mAb 3F10, (Roche) and peroxidase conjugated anti-biotin monoclonal antibody (Roche). Endogenous talin was detected with talin mAb 8d4 (Sigma).

For immunoprecipitation, cells were washed three times with HBSS, 1mM  $MgCl_2$ , 1 mM  $CaCl_2$  and  $2 \times 10^7$  cells in 1 ml were lysed with 2X lysis buffer (HBSS, 2% Triton X-100, 0.2% NP-40, 1 mM  $MgCl_2$ , 1 mM  $CaCl_2$ ), supplemented with proteinase inhibitors (Complete EDTA-free, Boehringer), incubated for 20 min on ice, and centrifuged at 14,000 rpm for 15 min. Supernatants were collected, 500  $\mu$ l aliquots were pre-cleared with 50  $\mu$ l of a 1:1 slurry of protein A agarose (Invitrogen) for 1 hour at 4 C, and then mixed with 3  $\mu$ g mAb CBR LFA-1/2 and 50  $\mu$ l protein A agarose for 1 hour at 4 C. The protein A beads were washed, heated at 100 C with SDS-sample buffer for 2 min, and eluates were subjected to SDS-PAGE.

Live cell staining for HA-tagged CXCR4 was performed at room temperature, incubating cells with anti-HA monoclonal antibody (12CA5, Roche) for 15 min and Cy5 conjugated anti-mouse Ig (Zymed) for 15 min.

### **V-Bottom Cell Adhesion Assay**

Cell adhesion was assayed as described (7, 34). Briefly, V-bottom 96-well plates (Corning) were coated with human tonsil ICAM-1 (6  $\mu$ g/ml in 20 mM Tris pH 9, 150 mM NaCl, 2mM MgCl<sub>2</sub>) or with 5  $\mu$ g/ml BSA as control at 4 °C overnight, and then blocked with 2% BSA for 1 hour at 37 °C. Cells were labeled with 2',7'-bis-(carboxyethyl)-5-(and -6)-carboxyfluorescein acetoxymethyl ester and resuspended in L15 medium/2.5% FCS. After incubation at 37 °C for 15 min, cells ( $7.5 \times 10^4$ ) were washed two times, allowed to recover for 5 min. at 37°C, and in 50  $\mu$ l of L15 medium / 2.5% FCS were added to ICAM-1-coated plates that had been pre-equilibrated to 37°C and contained 50  $\mu$ l/well of the same medium containing the indicated activating agents. The plates were immediately centrifuged at 200g for 15 min at room temperature. After centrifugation, nonadherent cells that accumulated at the center of the V-bottom were quantified by a fluorescence plate reader.

### **FRET Assay**

Imaging was performed with an Axiovert S100 inverted fluorescence microscope (Zeiss), equipped with Hamamatsu Orca digital CCD camera. Filters were from Chroma (Brattleboro, VT) and were YFP (D500/20X, 515DCLP, D535/30M), CFP (D436/20X, 455 DCLP, D480/30M), and Bleach (HQ535/60M, full reflective mirror, OG590LP), and Cy5 (D640/20X, 660DCLP, D680/30M). FRET image acquisition, image registration, background subtraction, and data analysis were performed with Openlab (Improvision,) software. Cells in culture (1 ml) were washed and resuspended with 1 ml L15 medium supplemented with 2 mg/ml D-glucose. Cells (250 or 500  $\mu$ l) were brought to a total volume of 1 ml with the same medium and allowed to settle and equilibrate for 10 min. at 37°C in a FCS2 live cell imaging chamber (Bioptechs). Activating agents (100x) were dropped onto the surface of the medium in the chamber in a 10  $\mu$ l drop. Pre-bleach FRET measurements were begun 10 min. later, or for PMA or SDF-1, 15 min. later. Cells were illuminated with a 100 W mercury arc lamp through a 50% ND filter and a

63x oil immersion objective lens. Exposure time was 0.5 sec for both CFP and YFP with 2 x 2 binning. Acceptor (YFP) photobleaching was done for 3 min without a ND filter using the bleach filter set, resulting in more than 95% reduction in the fluorescence intensity of YFP without direct effect on CFP intensity. The photobleached area included usually 4 to 5 cells which were present in each image set. Pre- and post-bleach image sets of both donor (CFP) and acceptor (YFP) were acquired. Individual cells in image sets showing significant drift in the focal plane were discarded. Typically each image set yielded data on 1 to 2 cells. After image registration and background subtraction, CFP signals in a ring outlining the cell membrane were selected as the region of interest.

FRET efficiency (E) was calculated as

$$E = 1 - (F_{\text{CFP}(d)_{\text{Pre}}} / F_{\text{CFP}(d)_{\text{Post}}}) \quad (35)$$

where  $F_{\text{CFP}(d)_{\text{Pre}}}$  and  $F_{\text{CFP}(d)_{\text{Post}}}$  are the mean CFP emission intensity prior to and following YFP photobleaching. A freshly prepared batch of cells was used for each photobleach experiment; typically 3 to 4 batches were required for each experimental condition. FRET values obtained from a separate analysis using the sensitized emission method (36) were in excellent agreement with those obtained using the photobleach method (data not shown).

## References

5. C. Lu *et al.*, *Proc. Natl. Acad. Sci. U. S. A.* **98**, 2387-2392 (2001).
6. P. E. Hughes *et al.*, *J. Biol. Chem.* **271**, 6571-6574 (1996).
7. C. Lu, T. A. Springer, *J. Immunol.* **159**, 268-278 (1997).
12. T. S. Ulmer, B. Yaspan, M. H. Ginsberg, I. D. Campbell, *Biochemistry* **40**, 7498-7508. (2001).
14. D. A. Zacharias, J. D. Violin, A. C. Newton, R. Y. Tsien, *Science* **296**, 913-916 (2002).
26. J. J. Campbell *et al.*, *Science* **279**, 381-384 (1998).
29. L. A. K. Teixeira, C. H. Fricke, C. B. Bonorino, M. R. Bogo, N. B. Nardi, *J. Biotech.* **88**, 159-165 (2001).
30. C. Huang, T. A. Springer, *J. Biol. Chem.* **270**, 19008-19016 (1995).
31. M. S. Hasson *et al.*, *Biochemistry* **37**, 9918-30 (1998).
32. B. Seed, *Nature* **329**, 840-842 (1987).
33. L. Petruzzelli, L. Maduzia, T. A. Springer, *J. Immunol.* **155**, 854-866 (1995).
34. M. Weetall *et al.*, *Anal. Biochem.* **293**, 277-287 (2001).
35. A. Miyawaki, R. Y. Tsien, *Meth. Enzym.* **327**, 472-500 (2000).
36. G. W. Gordon, G. Berry, X. H. Liang, B. Levine, B. Herman, *Biophys. J.* **74**, 2702-2713 (1998).